Scientific Research Publishing

Open Journal of Modern Hydrology, 2023, 13, 94-113
https://www.scirp.org/journal/ojmh
ISSN Online: 2163-0496
ISSN Print: 2163-0461

Sediment-Loading Processes in a Forested Catchment: Modeling and Observations

Md. Motaleb Hossain[1*], Kazuhisa A. Chikita[2], Yoshitaka Sakata[3]

[1]Department of Mathematics, Faculty of Science, University of Dhaka, Dhaka, Bangladesh
[2]Arctic Research Center, Hokkaido University, Sapporo, Japan
[3]Faculty of Geosciences and Civil Engineering, Institute of Science and Engineering, Kanazawa University, Kanazawa, Japan
Email: *motaleb313@yahoo.com

How to cite this paper: Hossain, Md.M., Chikita, K.A. and Sakata, Y. (2023) Sediment-Loading Processes in a Forested Catchment: Modeling and Observations. *Open Journal of Modern Hydrology*, **13**, 94-113.
https://doi.org/10.4236/ojmh.2023.132005

Received: December 2, 2022
Accepted: January 31, 2023
Published: February 3, 2023

Abstract

In order to investigate sediment-loading processes in a catchment, the daily time series of river discharge and sediment load were applied to a semi-distributed model, the Soil and Water Assessment Tool (SWAT). The time series of discharge and sediment load were obtained by monitoring the river stage and water turbidity of the Oikamanai River, Hokkaido, Japan, in the rainfall season (April-November) of 2011-2014. The catchment is forested (ca 90% area) but underlain by the Neogene sedimentary rocks with currently active faults and forest soils with tephra layers, which tend to frequently produce slope failure such as landslide and bank collapse by rainfall or snowmelt. The water turbidity, T, in ppm was converted into suspended sediment concentration, SSC, in g/L by applying the linear relationship between T and SSC. The acquisition of the time series of discharge, Q (m^3/s) and sediment load, L (=Q·SSC in g/s) of the river allowed us to distinguish the fluvial sediment transport, accompanied by slope failure in the upstream, from that under no slope failure. The SWAT was used to simulate soil erosion and identify the region prone to the soil erosion in the Oikamanai River basin. The model's results showed a satisfactory agreement between daily observed and simulated sediment load as indicated by the high Nash-Sutcliffe efficiency. This evidences that the upper mountainous region of the catchment provides a main sediment source, accompanied by slope failure.

Keywords

SWAT, Slope Failure, Landslide, Bank Collapse, Forested Catchment, Sediment Load

1. Introduction

The slope failure in this study means the surface failure and deep landslide on

catchment slope and the bank collapse in riparian regions, which occur under rainfall, snowmelt or earthquake. Landslides mechanism and the dynamic processes of landslides have been investigated by many geologists, geomorphologists and geophysicists [1] [2], but studies on subsequent fluvial sedimentation processes, connected to river sediment load, are very few in the world [3]. Fluvial sediment has been measured using the concentration of suspended sediment [4]. The acquirement of discharge and suspended sediment concentration time series in a river allow us to explore the source location, availability and loading processes of sediment in the catchment [5] and to simulate long-term sediment yield or sediment load by modelling [6] [7]. Neogene sedimentary rock tends to have high frequency of landslide, compared with metamorphic rocks, Mesozoic and Paleozoic rocks and volcanic rocks [8]. It is because the Neogene sedimentary rock is relatively soft, and thus easily receives the weathering. In case of the Oikamanai River catchment, the Neogene sedimentary rock is also accompanied by active faults. These make us focus on the hydrological role of fractures or faults in groundwater flow system. Several adverse economic and environmental impacts due to the damaging effects of soil erosion have been reported. Our study area, the Oikamanai River catchment, eastern Hokkaido, is forested (ca. 90% area), but accompanied by two tephra layers (Tarumae Ta-b in 1667 and Shikotsu Spfa-1, 40,000 years ago) in forest soils and the Neogene sedimentary rocks with active faults, which tend to frequently produce surface failure and deep landslide respectively, under heavy rainfall or snowmelt. The tephra layers in forested area are protected from slope failure by tree roots, but bank collapse easily occurs in riparian region of this forested catchment. In order to understand and predict such disastrous phenomena and subsequent fluvial sedimentation in the catchment, we monitored water level and water turbidity in the Oikamanai River catchment in rainfall seasons of 2011-2014 to identify sediment sources and sediment loading processes by exploring the feature of discharge and sediment load variations and modeling the two-time series. Estimating sediment sources like as SWAT model researchers use Global Assessment of Soil Degradation (GLASOD) mapping [9]. The sediment yield estimation model used in this study is the SWAT model. It is a semi distributed comprehensive processed based model for simulating water, sediment and chemical fluxes in catchments under varying climatic conditions, soil properties, stream channel characteristics, land use and agricultural management [10] [11]. The SWAT model has been applied to enhance the understanding of sediment loss and transport process over a wide range of environments around the world [12]. For modeling the sediment yield, Mukundan *et al.* [13] examined the suitability of SWAT at the North Fork Broad River catchment, and their results suggested that the SWAT model is a better substitute than the sediment rating curve for estimating sediment yield. Many researchers have reported that the SWAT model predicted reasonable results for sediment yield estimation when accurate input data and model parameterization are provided [14] [15]. Here, we have

aimed to identify the sediment sources in the Oikamani River basin by applying the observed daily mean discharge and sediment load time series to the SWAT model. The turbidity and river-stage monitoring were performed at two sites along the river, and thereby, we distinguished the sediment yield in the upstream or downstream region of the catchment, and identified the seasonal sediment source in the upper catchment, since more slope failure or the runoff events accompanied by higher sediment yield occur in the upper catchment. The monitoring at the two sites also revealed that the net sediment deposition occurs between the two sites which is coincide with simulated result. SWAT model can be used to estimate the sediment deposition where direct measure of sediment concentration is not possible.

2. Study Area

The forested Oikamanai River catchment in the Tokachi district of southeastern Hokkaido, Japan (**Figure 1**) [16] [17] (42˚33'46"N to 42˚40'40"N, 143˚21'47"E to 143˚28'36"E; altitude, 6 m to 330 m asl) upstream of site R1 has the area of 62.47 km^2, the mean slope angle of 17˚ and the mean riverbed gradient of 0.033 (**Figure 2**) [18]. The digital elevation model (DEM) in **Figure 1** is made up by 0.1 km × 0.1 km mesh. The distribution of slope angle corresponds to that of the surface geology (**Figure 2**); the upper, middle and lower regions with relatively steep slope in the northwest to southeast directions are occupied by sedimentary rocks of early to middle Miocene, middle to late Miocene and late Miocene to Pliocene, respectively, and the lowest region with relatively gentle slope just upstream of site R1 by alluvial flood deposits. The sedimentary rocks are composed of conglomerate, sandstone, mudstone, siltstone and tuff. The Neogene sedimentary rock as in the Oikamanai River catchment tends to have high frequency of landslide, compared with metamorphic rock, Mesozoic and Paleozoic rocks and volcanic rocks. It is because the Neogene sedimentary rock is relatively soft, and thus easily receives the weathering. The sedimentary rocks in the mountainous regions are accompanied by many faults, which are due to the orogenic movement of the Hidaka Range at ca. 45 km southwest of the catchment. The northern faults are currently active, producing the high sediment yield from landslide or bank collapse in the mountainous region (Tokachi Subprefecture HP; URL, http://www.tokachi.pref.hokkaido.lg.jp/sr/srs/gaiyou/sugata/sugata.htm) (**Figure 2**). Sandy pyroclastic deposits of late Pleistocene are distributed on the catchment slope, connected to the area along the border of flood plain and forest regions. Such permeable deposits could make the seepage easy from the forest region to the flood plain. According to the Hjulström curve, such sandy deposits are easily eroded by overland flow or river flow. The catchment upstream of site R1 is covered by 88.3% forest in the mountainous region, 10.6% farmland (mostly, grassland) on the lowest alluvial plain and others. The forest is composed of ca. 50% broad-leaved and ca. 50% coniferous (mainly, Sakhalin fir; *Abies sachalinensis*) trees.

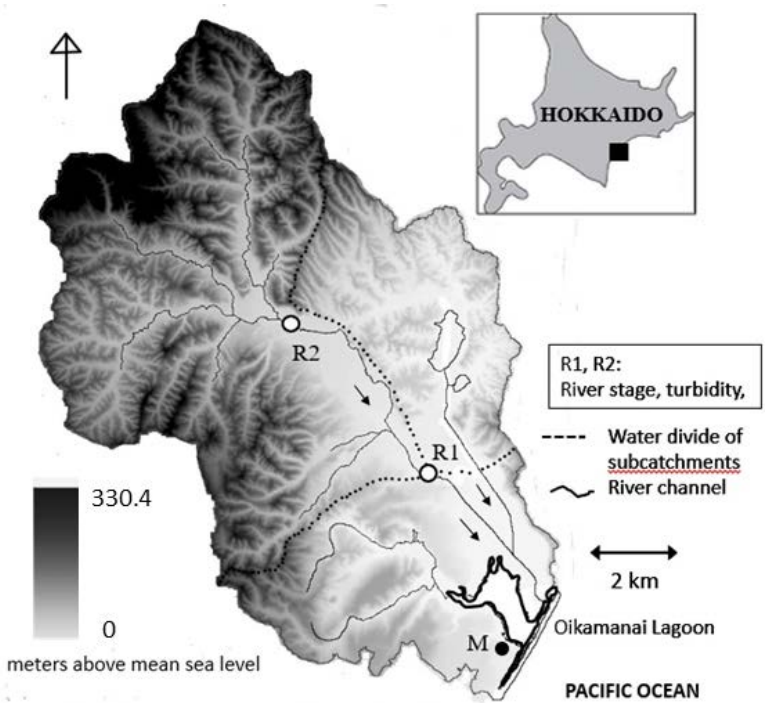

Figure 1. Location of the Oikamanai River catchment in eastern Hokkaido, Japan, and observation sites in the catchment, shown by the digital elevation model (DEM). At site M, rainfall and air temperature were measured.

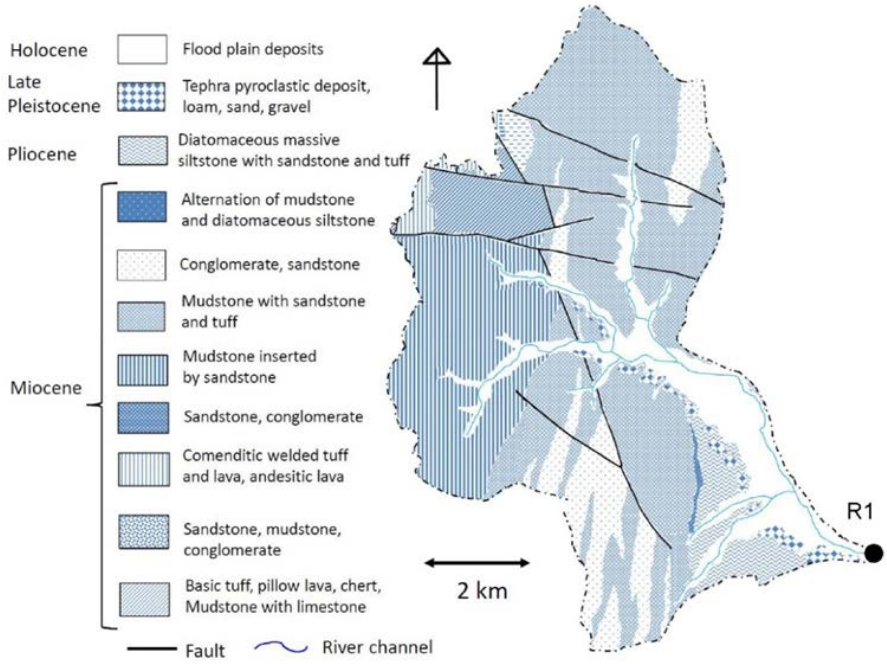

Figure 2. Geology of the catchment upstream of site R1 [18].

3. Methodology

3.1. Instrumentation and Sampling

The monitoring of water level, air temperature, water temperature and water tur-

bidity at site R1 was performed at 1 hour intervals by HOBO air pressure and water pressure loggers with temperature sensors (Onset Computer, Inc., USA; the range of 69 - 207 kPa and the accuracy of ±0.62 kPa for pressure, and the range of −20˚C to 50˚C and the accuracy of ±0.2˚C for temperature), and a self-recording Turbidimeter of infrared back-scattering type with a window-cleaning wiper (type ATU3-8 M, Advantech, Inc., Japan, with a range of 0 - 20,000 ppm and an accuracy of ±20 ppm), respectively, in April 2011-November 2014 (Figure 1). At site R2 ca. 6 km upstream of site R1, the same instruments were similarly fixed in April 2013-November 2014. Instantaneous turbidity (ppm) was measured ten times at 1 sec interval every 1 hour and averaged for the 10 samplings. The averaged turbidity was converted into suspended sediment concentration (SSC; mg/L) from simultaneous water samplings by a depth-integrating sampler (Figure 3). Two regression lines with a boundary at 200 ppm were acquired, since relations between electric signal and turbidity are obtained at 0 - 200 ppm and 200 - 20,000 ppm in manufacture, using suspension of kaolin powder.

Water level, h (m), at site R1 and site R2 was changed into river discharge, *Q*

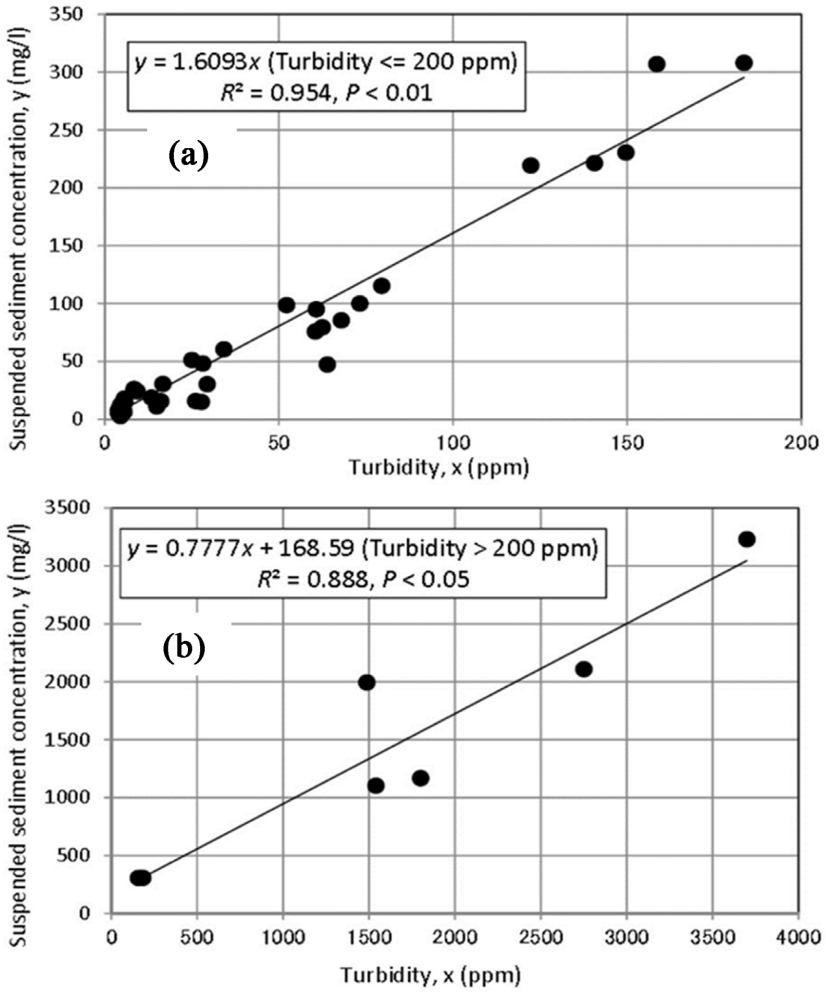

Figure 3. Relationships between water turbidity (ppm) and suspended sediment concentration (SSC: mg/L), (a) turbidity ≤ 200 ppm, (b) turbidity > 200 ppm.

(m^3/s), by the different h—Q rating curves which was obtained by measuring discharge several times per year and by applying the Manning equation to the channel cross-section at sites R1 and R2 (**Figure 1**). The Oikamanai River channel is artificially regulated by concrete blocks constructed in 1996. However, riverbed configuration could change to a degree by sediment deposition or erosion in the river channel. Hence, we have used four different rating curves to measure discharge at sites R1 and R2. The sediment load, L (kg/s), was calculated by L = SSC·Q, where SSC is suspended sediment concentration (g/L). The forest soil is most permeable at depths of 30 – 40 cm, indicating the high hydraulic conductivity of $K_s = 1.7 \times 10^{-2}$ cm/s [19]. The high hydraulic conductivity is due to the inclusion of gravels, although the percentage of silt and clay is similar to that in the lower much less permeable layer ($K_s = 1.8 \times 10^{-5}$ cm/s at 40 - 50 cm depth). The gravels probably originate in tephra pyroclastic deposits from volcanic eruptions in the Holocene. Thus, the downslope subsurface flow could occur in the highly permeable layer during rainfall or snowmelt, because the vertical percolation is interrupted by the much less permeable soil layer at 40 - 50 cm depth. The grassland soil is impermeable except for the sandy layer of 0 - 20 cm at $K_s = 1.4 \times 10^{-3}$ cm/s, which is equivalent to the infiltration capacity at 5.0 mm/h. The grassland on the flood plain between soil sampling site and site R1 could produce the subsurface flow only in the surficial soil layer, and, at rainfalls of more than 5.0 mm/h, also the Hortonian overland flow, of which the rainfalls occurred a few times in 2011-2014.

The weather data were obtained at site M (rainfall and air temperature) near the Oikamanai Lagoon [16] [17] at 4.0 km south-southeast of site R1, and at two weather stations, the Bisei weather station (precipitation, air temperature, solar radiation, and wind speed and direction) 9.6 km south of site R1 and the Taiki-town weather station (snow depth, precipitation, air temperature, and wind speed and direction) 18.9 km southwest of site R1. The distinction between rainfall and snowfall in the catchment was performed under air temperature more than 2˚C at site M (altitude, 6 m asl).

3.2. SWAT Model Description

Soil and Water Assessment Tool (SWAT) model is used to simulate the discharge and sediment load time series. The SWAT is a physical process based semi-distributed model to simulate continuous-time landscape processes at a catchment scale [20] [21]. The catchment is divided into different subbasins, and the subbasins are divided into different hydrological response units (HRUs) based on soil type, land use and slope classes giving a high level of spatial detail simulation. The Oikamanai River basin is divided three subbasins (**Figure 4(a)**) and the subbasins are divided into 29 HRUs. The major model components include hydrology, weather, soil erosion, nutrients, soil temperature, crop growth, pesticides agricultural management and stream routing. The model predicts the hydrology at each HRU using the water balance equation, which includes daily precipitation, runoff, evapotranspiration, percolation and return flow compo-

nents. The surface runoff is estimated in the model using two options 1) the Natural Resources Conservation Service Curve Number (CN) method [22] (USDA-SCS, 1972) and 2) the Green and Ampt method [23]. The percolation through each soil layer is predicted using storage routing techniques combined with crack-flow model [24]. The evapotranspiration is estimated in SWAT using three options 1) Priestley-Taylor [25], 2) Penman-Monteith [26] and 3) Hargreaves [27]. The flow routing in the river channels is computed using the variable storage coefficient method [28] or Muskingum method [29]. In a conservative environment, the total water entering channels every day from each HRU in the SWAT model can be derived from

$$Q_{flow} = \left(Q_{surf} + Q_{lat} + Q_{gw}\right) \cdot HRU_{area} \tag{1}$$

where Q_{flow} is the total water entering the channel of the subbasin where the HRU is located (mm^3), Q_{surf} is surface runoff yield (mm), Q_{lat} is lateral flow yield (mm), Q_{gw} is groundwater yield (mm) and HRU_{area} is the HRU area (mm^2). The SWAT model uses the Modified Universal Soil Loss Equations (MUSLE) to compute HRU-level soil erosion. The modified universal soil loss equation (MUSLE) [30] to compute soil erosion on the catchment slope is

$$Sed = 11.8\left(Q_{surf} \cdot q_{peak} \cdot area_{hru}\right)^{0.56} \cdot K_{USLE} \cdot C_{USLE} \cdot P_{USLE} \cdot CFRG \tag{2}$$

where Sed is the sediment load on a given day(metric tons), Q_{surf} the surface runoff volume (mmH_2O/ha), q_{peak} s the peak runoff rate (m^3/s), $area_{hru}$ is the area of the HRU(ha), K_{USLE} s the USLE soil erodibility factor, C_{USLE} s the USLE cover and management factor, P_{USLE} s the USLE support practice factor, LS_{USLE} the USLE topographic factor and CFRG is the coarse fragment factor. The MUSLE uses runoff energy to detach and transport sediment [31]. The sediment routing in the channel consists of channel degradation using stream power [32] and deposition in channel using fall velocity. Channel degradation is adjusted using USLE soil erodibility and channel cover factors.

3.3. SWAT Model Input

In this study, the inputs required by the SWAT model are daily weather data for precipitation, maximum and minimum temperature, wind speed, solar radiation and relative humidity, which were obtained from the weather stations' records (**Figure 1**) from 2008 to 2014. Digital elevation model (DEM) data upstream of site R1 (**Figure 4(a)**) was prepared using a digital map with a 30 m grid elevation created from a 1:25,000 topographic map published by the Japanese Geographical Survey Institute (GSI, http://nlftp.mlit.go.jp/ksj/jpgis/jpgis_datalist.html). GIS-referenced soil data (**Figure 4(c)**) were extracted from a 1:50,000 soil map of the Fundamental Land Classification Survey developed by the Hokkaido Regional Development Bureau (https://www.naro.go.jp/english/topics/laboratory/niaes/074998.html). A land use map (1:25,000) based on land cover in 2005 was obtained from the GSI (**Figure 4(b)**).

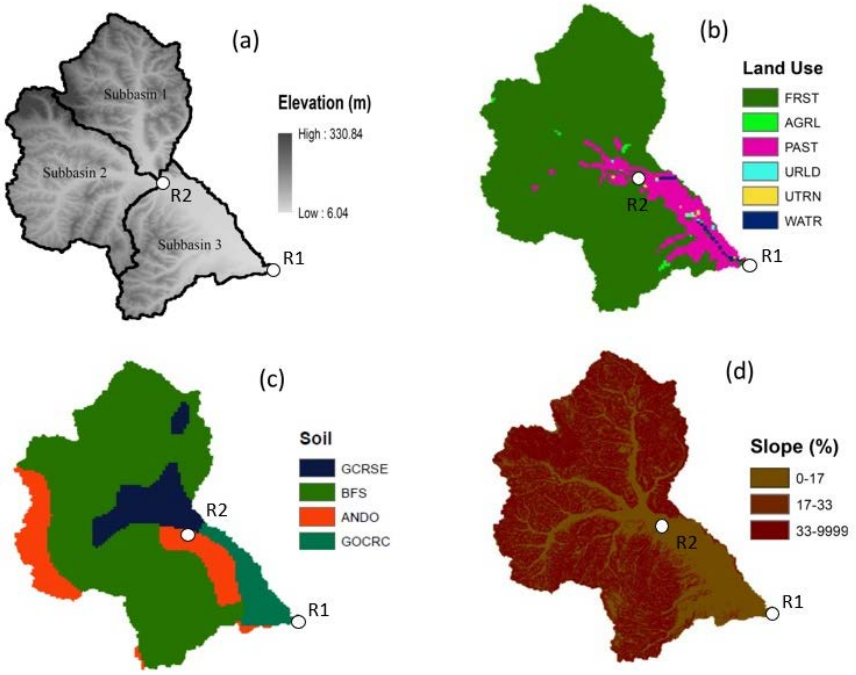

Figure 4. (a) Digital elevation map, (b) Land use, (c) Soil, (d) Slope classes of Oikamanai River basin with observation sites, R1 and R2.

The Oikamani River catchment is covered by six types of land (**Figure 4(b)**), and is mostly occupied by forest (FRST) (88.3%) and farmland (PAST) (10.6%). The farmland is mainly grass land area. Four types of soil are distributed in this study area where main soil is brown forested soil (BFS) (67.99%) (**Figure 4(c)**) followed by ando (ANDO) (12.90%) and gley soil; in the gley soil, there are two types, gley coarse (GCRSE) (12.70%) and gley ochric (6.40%). The catchment thus exhibits the land use and soil dominated by forest and brown forested soil, respectively.

3.4. Model Performance Evaluation

The acceptance of SWAT simulation results is determined by examining the Nash and Sutcliffe efficiency (ENS) [33] and relative error (R_e). The ENS simulation coefficient indicates how well the plot of observed values versus simulated values fits the 1:1 line. If the ENS value is less than or very close to zero, the model prediction is unacceptable or poor. If the values are one, then the model prediction is perfect [34]. R_e also indicates how close the observed values versus the simulated values are. R_e can range from zero to a very large value, with zero representing perfect agreement between the model and real data. Essentially, when the model efficiency R_e and ENS are close to one, and when the model efficiency R_e is close to zero, the models are considered more accurate. The ENS is defined in the following:

$$ENS = 1 - \frac{\sum_i^n \left(X_{obs,i} - X_{model,i} \right)^2}{\sum_i^n \left(X_{obs,i} - \bar{X}_{obs} \right)^2} \quad (3)$$

The root mean squared error (RMSE) of a model prediction with respect to the estimated variable $X_{model,i}$ is defined as follows:

$$RMSE = \sqrt{\frac{\sum_i^n \left(X_{obs,i} - X_{model,i}\right)^2}{n}} \quad (4)$$

where $X_{obs,i}$ is the observed data on day *i*, $X_{model,i}$ is the simulated output on day *i*, $\bar{X}_{obs}$ is the average measured value during the study period.

3.5. Model Calibration and Validation

The SWAT model was first calibrated using SWAT Calibration and Uncertainty Programs (CUP) with the Sequential Uncertainty Fitting (SUFI2) calibration and uncertainty analysis routine [35]. The calibration of flow and sediment was then performed manually to obtain a good match between the observed and simulated values. Key hydrological and sediment-related parameters were selected from sensitivity analysis. Calibration is an effort to better parameterize a model to a given set of local conditions, thereby reducing the prediction uncertainty. Model calibration is performed by carefully selecting values for model input parameters by comparing model predictions for a given set of conditions with observed data for the same conditions. Model validation is the process of demonstrating that a given site-specific model is capable of making sufficiently accurate simulations. The validation involves running a model using parameters that were determined during the calibration process, and comparing the predictions to observed data not used in the calibration. The calibration and validation are typically performed by splitting the available observed data into two datasets: one for calibration, and another for validation, data are most frequently split by time periods [36]. In this study, parameters calibrated for stream flow are shown in Table 1. Sensitive parameters are calibrated within their acceptable ranges to match the simulated streamflow with the observed streamflow (Table 1). Snow

Table 1. Parameters for streamflow calibration performed at site R1 of the Oikamanai River catchment in 2012.

No.	Parameters	Definition of Parameters	Fitted values
1	r_CN2.mgt	Initial SSC runoff curve number for moisture condition	0.72
2	v_CH_K2.rte	Effective hydraulic conductivity in main channel alluvium (mm/h)	17.62
3	r_SOL_AWC.sol	Available water capacity of the soil layer	−0.94
5	v_GWQMN.gw	Treshold depth of water in the shallow aquifer required for return flow to occur (mm)	830.11
6	v_REVAPMN.gw	Threshold depth of water in the shallow aquifer for “revap” to occur (mm)	521.53
7	v_ESCO.hru	Soil evaporation compensation factor	0.99
8	v_SURLAG.bsn	Surface run off lag time	11.94
9	v_ALPHA_BF.gw	Baseflow alpha factor (days)	0.99
11	v_EPCO.hru	Plant uptake compensation factor	0.01
12	v_RCHRG_DP.gw	Deep aquifer percolation fraction	0.86

depth in 2012 is nearly two times of 2011; it indicates that initial condition of soil water content, groundwater storage, and soil parameters are different in different years. Hence, we have simulated year-wise discharge, which occurs for a single year of non-snowfall and non-snowmelt seasons taken for calibration and the other years taken as validation periods. The period of April–November 2012 is considered for calibration and the periods of April–November 2011, 2013 and 2014 for validation (Figure 6). The calibrated parameters in 2012 are showed in Table 1. Here the parameters are calibrated within their acceptable ranges to match the simulated streamflow. In the year 2012 the most sensitive parameter is runoff curve number (CN2.mgt) followed by effective hydraulic conductivity in main channel alluvium (mm/h) (CH_K2.rte), available water capacity of the soil layer (SOL_AWC.sol), and maximum canopy storage (CANMX.hru) etc. (Table 1).

4. Results and Discussion

4.1. Observed Data

Figure 5 shows hourly time series of water temperature, discharge, suspended

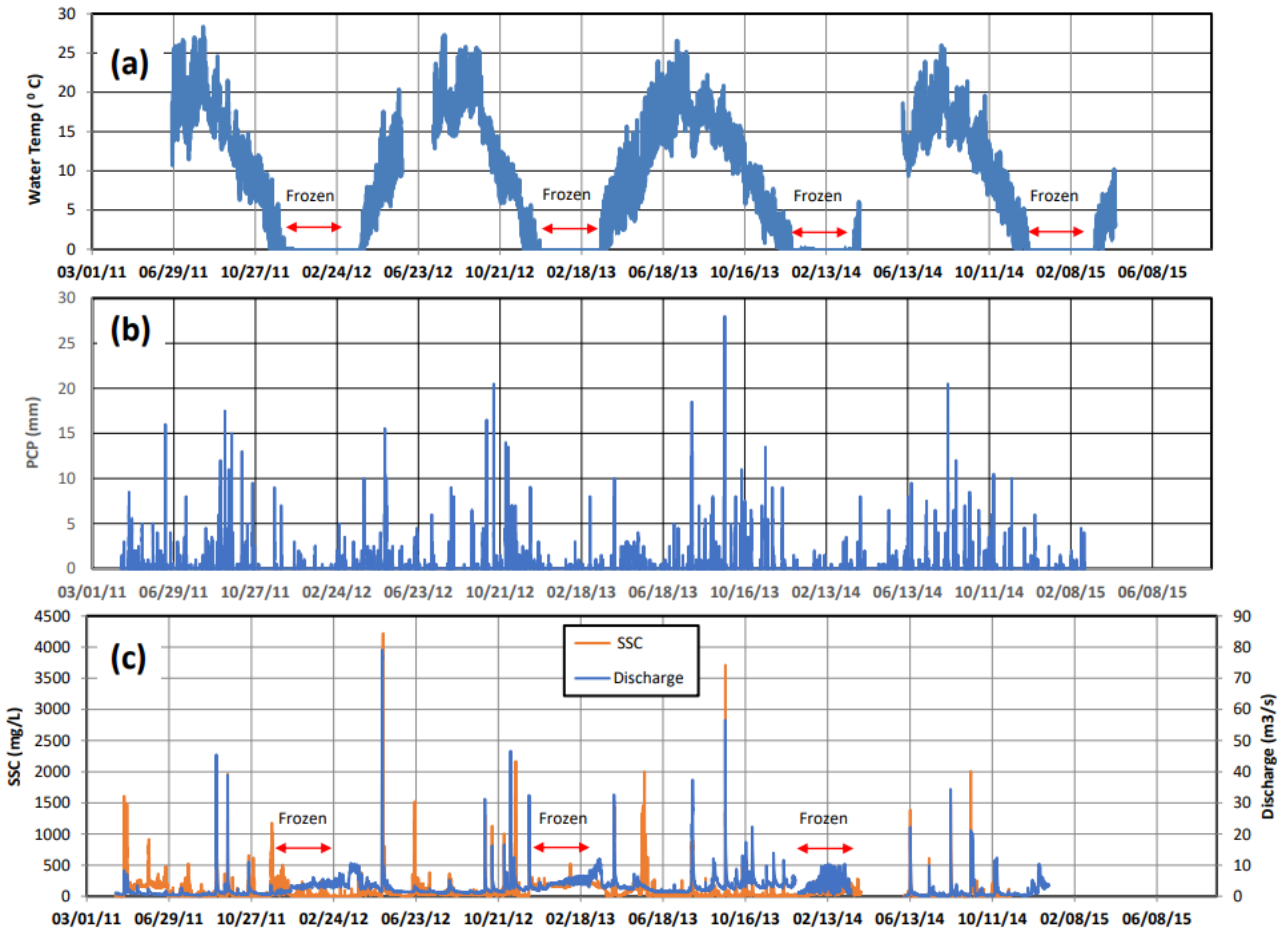

Figure 5. Hourly time series of (a) water temperature, (c) discharge and suspended sediment concentration (SSC) at site R1, and (b) precipitation at the Bisei weather station since April 2011. The arrows with the label "Frozen" indicate the completely ice-covered periods of the Oikamanai River.

sediment concentration (SSC) at site R1 and precipitation at the Bisei weather station in April 2011-November 2015. As shown by water temperature at ca. 0˚C, the Oikamanai River was frozen down to the depth of the pressure logger in mid-December-March every year. The rating curve of discharge and suspended sediment concentration was then not applicable, because the covered-ice growth and snow accumulation on the ice substantially increases the water pressure recorded. As a result, the accurate observation of snowmelt runoffs in the snowmelt season was difficult, because snowmelt water then flew on the covered ice. Hence, only rainfall river runoff events under ice or snow-free condition are here discussed. When water temperature varied at more than 0˚C (Figure 5(a)), both discharge and SSC varied in response to rainfall (Figure 5(b) and Figure 5(c)). Especially, there was a strong correlation between rainfall and discharge.

4.2. Discharge Simulation

We have acquired discharge and sediment concentration data for non-frozen periods (April-November) of 2011-2014. Here the SWAT model was applied for year-wise non-frozen periods. The year 2012 (Figure 6(a)) data was provided for calibration and the data of the other years 2011 (Figure 6(b)), 2013 (Figure 6(c))

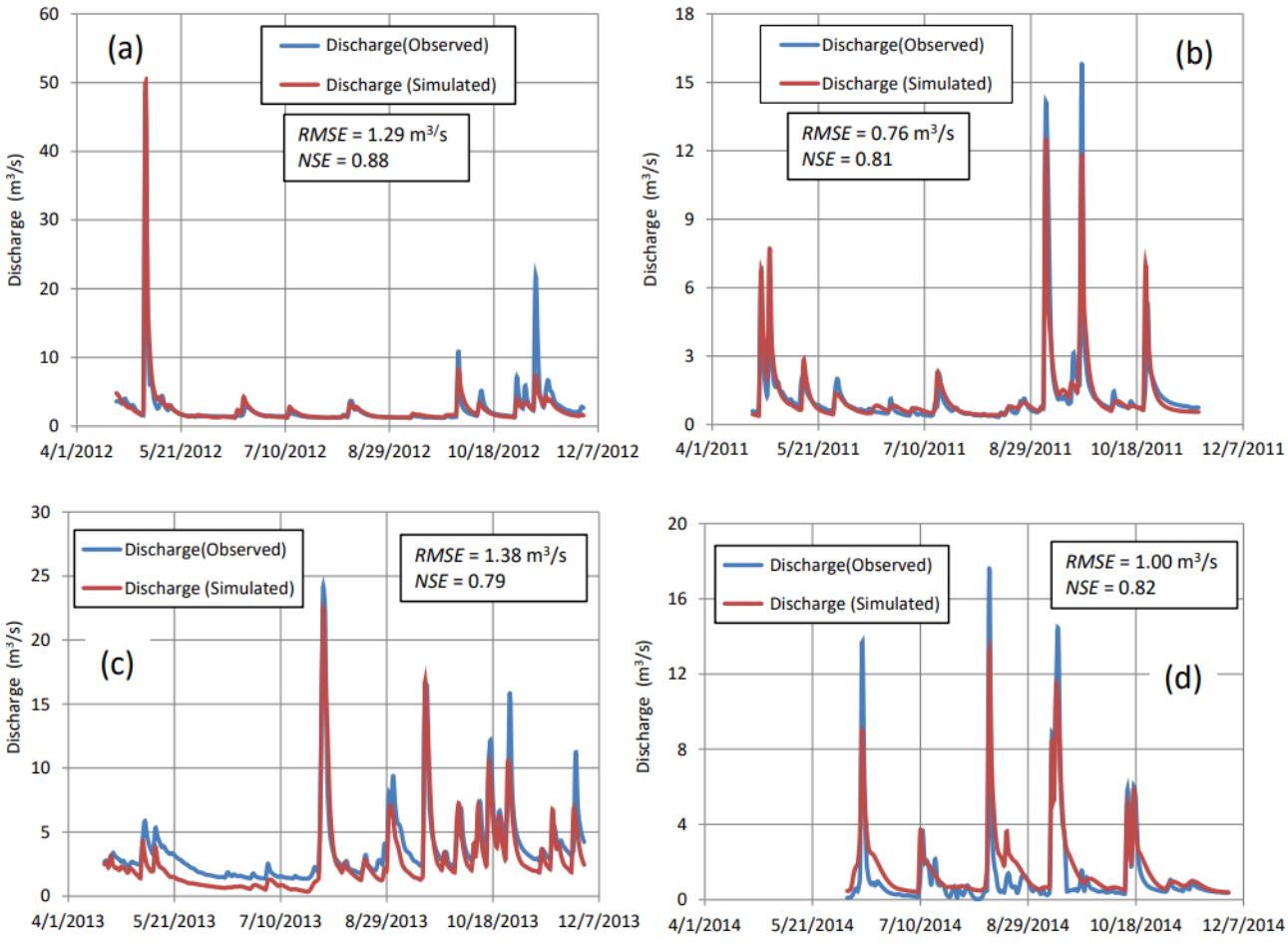

Figure 6. Discharge simulations at site R1. (a) Calibration in 2012, and validations in (b) 2011, (c) 2013 and (d) 2014.

and 2014 (Figure 6(d)) were utilized for validation. We have selected 12 sensitive parameters after sensitivity analysis for discharge simulation. The sensitive parameters and their calibrated values are shown in Table 1. Figure 6 graphically illustrates the comparison between the observed and simulated daily discharge at the main outlet R1 of the Oikamanai River catchment. The statistical performance of the SWAT for daily streamflow estimation gave satisfactory NSE values in the calibration year 2012 at 0.88 and in the validation 2011, 2013 and 2014 years at 0.81, 0.79 and 0.82, respectively. However, the simulated peak discharge was overestimated in early May of the calibration year 2012, because the heavy rainfall event affected the whole model simulation. To reduce the modeled discharge in this event of 2012, the calibration process changed some parameters values which affected the validation period by underestimated peak discharged during some heavy rainfall periods in Figures 6(b)-(d). In addition, the precipitation duration and intensity are possibly not considered by the soil conservation services (SCS) curve number (CN) method (SCS, 1972) for simulation of streamflow in SWAT model as reported by Phomcha *et al.* [37]. This limitation might be more serious for the simulation of heavy rainfall events.

4.3. Sediment Load Simulation

The SWAT model is further applied to sediment yield calibration following completion of discharge calibration process in the years 2011, 2012, 2013 and 2014. The sediment load simulation is rather difficult, because the sediment can originate from basin slope, slope failure (bank collapse and land slide), river bank erosion or river bed erosion. Here we have simulated the sediment load time series for each of the years 2011-2014 (Figure 7). Table 2 presents the calibrated parameters for sediment simulation in each year. Figure 7 generally indicates that the simulated daily sediment loads of the SWAT model and the observed values are comparable in magnitude, yielding NSE of 0.74, 0.91, 0.75 and 0.76 in the years 2011, 2012, 2013 and 2014, respectively. However, a comparison of the results indicates that the SWAT model could overestimate the sediment load for some high-flow events (Figure 7(b)), because, in the time period of heavy rainfall, the SWAT model makes all the soils eroded by runoff reach the river channel directly without considering sediment deposits remaining on surface catchment areas. The results also indicate that the SWAT model underestimated the sediment load of some peak events in Figure 7(a), Figure 7(c) and Figure 7(d). It is probably because landslide and bank collapse are not considered and the sediment routing algorithm used in SWAT is very simplified. The topographic factor (LSUSLE) automatically estimated from the DEM in the SWAT model proved to contain errors [38] [39], which partially explains the model inaccuracies for sediment yield estimation. Together with better accuracy and resolution of DEM, more reliable methods are needed for derivation of the topographical variables related to LSUSLE, such as the slope. The most sensitive parameters for sediment load simulation were the land cover and management

Table 2. Optimum values of sediment parameters in SWAT.

No.	Parameters	Definition of Parameters	2011	2012	2013	2014
1	USLE_C(FRST).crop.dat	Forest land cover and management factor	0.27	0.01	0.22	0.01
2	USLE_C(PAST).crop.dat	Farmland cover and management factor	0.17	0.73	0.24	0.14
3	USLE_P.mgt	USLE support practice factor	0.04	0.42	0.17	0.88
4	SPCON.bsn	Linear sediment reentrained parameter for channel routing	0.01	0.01	0.01	0.00
5	SPEXP.bsn	Exponent sediment reentrained parameter for channel routing	1.38	1.29	1.34	0.97
6	ADJ_PKR.bsn	Peak rate adjustment factor in the tributary channel	1.59	1.16	0.79	0.53
7	PRF.bsn	Peak rate adjustment factor in the main channel	1.73	1.91	1.05	0.96
8	CH_COV1.rte	Channel erodibility factor	0.17	0.17	0.29	0.32
9	CH_COV2.rte	Channel cover factor	0.66	0.86	0.72	0.83
10	USLE_K.sol	Soil erodibility factor	0.03	0.02	0.33	0.12
11	CH_BNK_BD.rte	Bulk density of channel bank sediment	1.48	1.84	1.60	1.69
12	CH_BED_BD.rte	Bulk density of channel bed sediment	1.63	1.89	1.76	1.82

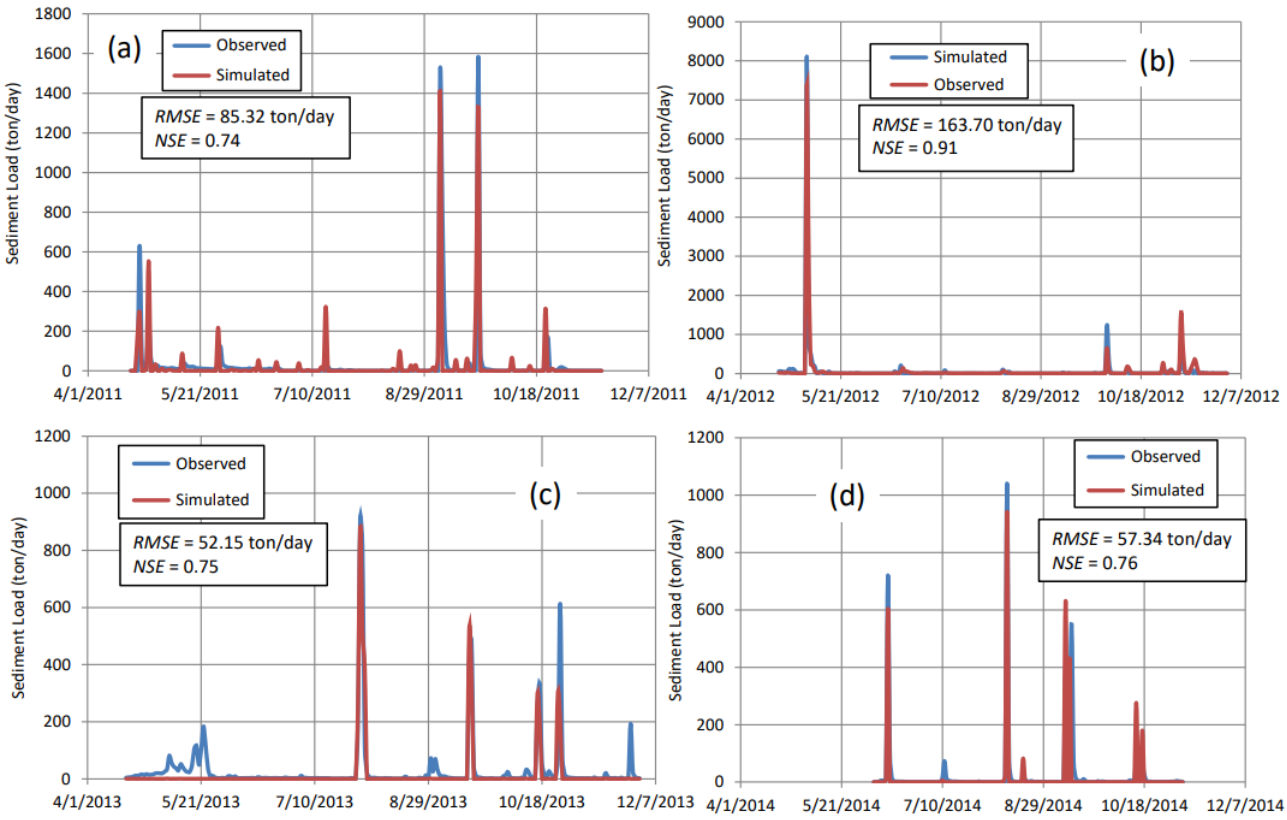

Figure 7. Sediment load simulation at site R1 in (a) 2011, (b) 2012, (c) 2013 and (d) 2014.

factor (USLE _C (FRST), USLE _C (FRST)), the USLE equation support practice factor (USLE_P.mgt), the peak rate adjustment factor (PRF.bsn, ADJ_PKR.bsn) and the soil erodibility factor (USLE_K.sol). Other parameters were nearly con-

stant in the whole four years (Table 2).

4.4. Comparison of Discharge and Sediment Load between Site R1 and Site R2

Here, the temporal variations of discharge and sediment load are compared between site R1 and site R2 (Figure 1). The data failure was occurred in snow fall and snowmelt periods and in April-June 2014. Thus, the discharge, sediment load and sediment yield are not continuous as shown by Figures 8-10. Observed daily discharge at site R1 was similar to that at site R2 for relatively large discharge peaks, but larger than that at site R2 for the lower discharge peaks (Figure 8). This is probably due to the nearly even or uneven distribution of rainfall in the catchment; in the former case, the rainfall probably became large especially in the region upstream of site R2, and in the latter case, the rainfall was relatively even over the catchment or relatively large in the lower region.

Meanwhile, the sediment load at site R2 was always greater than that of site R1 (Figure 9), though the discharge at site R1 was comparable to or larger than at site R2 (Figure 8). The sediment load at site R2 could occur on the relatively steep slope upstream of site R2 with the surface geology of mostly Neogene sedimentary rocks in subbasin 1 and subbasin 2 (Figure 1, Figure 2 and Figure 4(a)), which could frequently produce landslides by heavy rainfalls or snowmelt.

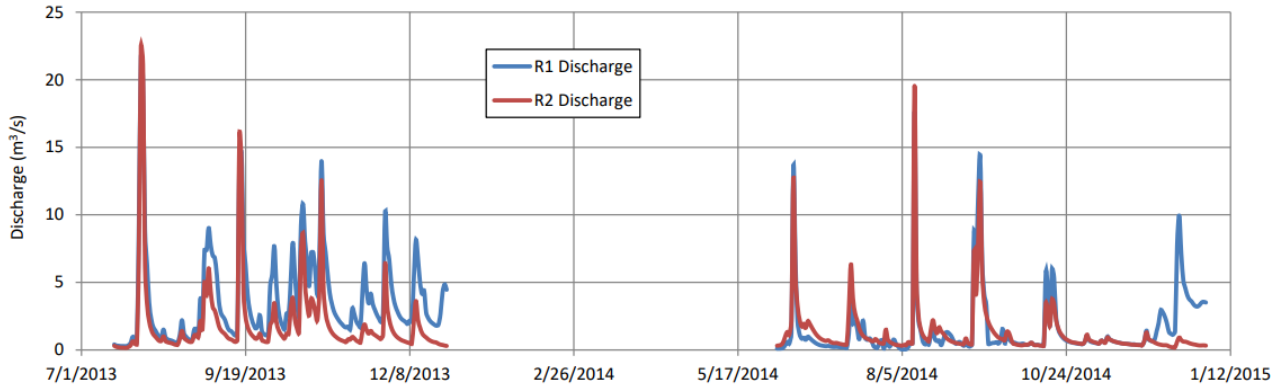

Figure 8. Daily observed discharge at sites R1 and R2.

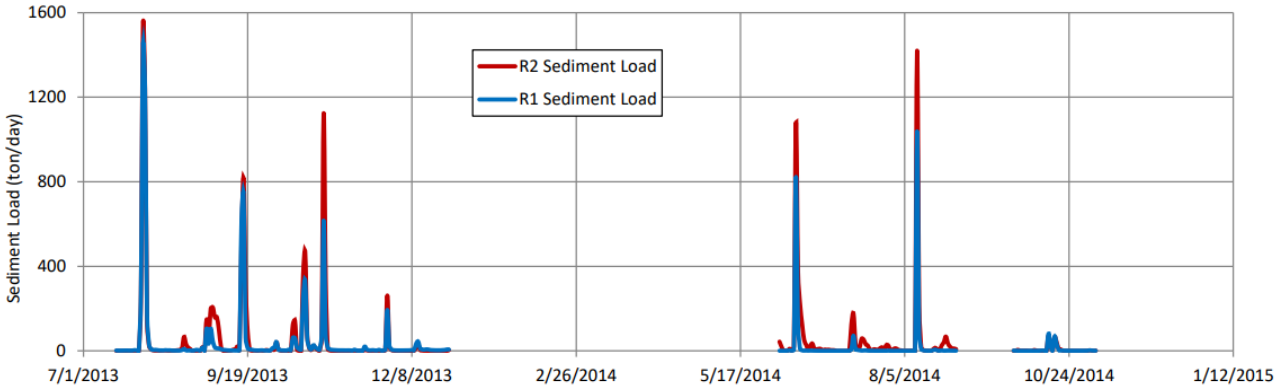

Figure 9. Sediment load at site R1 and site R2.

Also, the forest soils are accompanied by permeable tephra layers of Tarumae Ta-b and Shikotsu Spfa-1, easily producing surface failure.

Figure 10 shows the sediment yield (ton/day/km^2) at site R2 and site R2. The sediment yield at site R2 was always greater than that of site R1. This means that transportation of sediment at site R1 is less than at site R2. The sediment yield calculated between site R1 and site R2 is shown in Figure 11. It is seen that the sediment yield between site R1 and site R2 is negative in most of the events. This means that the sediment input at site R2 is larger than the sediment output at site R1, indicating that the sediment deposition occurred between site R2 and site R1. This is also caused by relatively steep slope upstream of site R2 (Figure 1), where the Neogene sedimentary rocks with active faults are distributed, more frequently producing landslide and bank collapse under rainfall. The region between site R1 and site R2, accompanied by relatively gentle slope, is composed of flood plain deposit of Holocene. Also, the lower region is covered mainly by

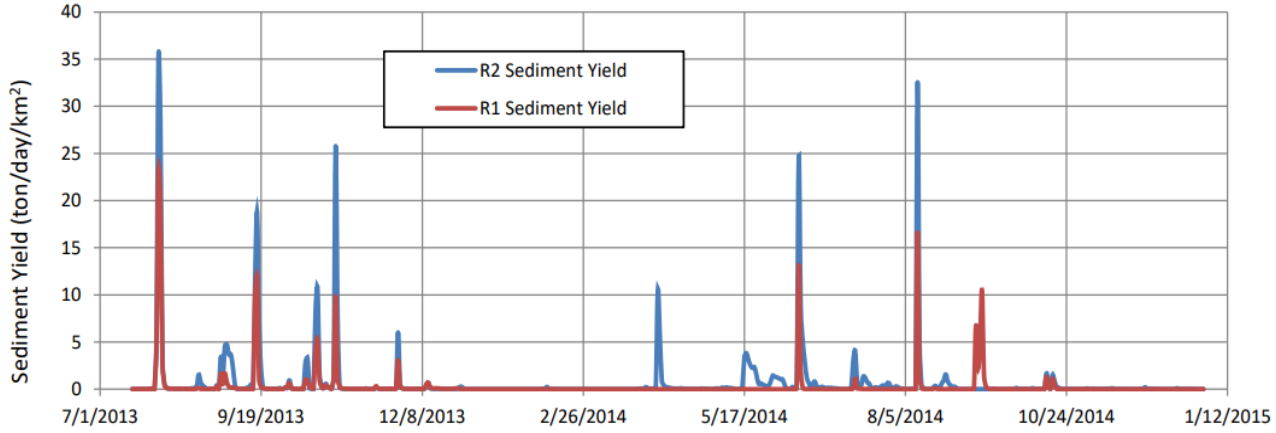

Figure 10. Sediment yield at site R1 and site R2.

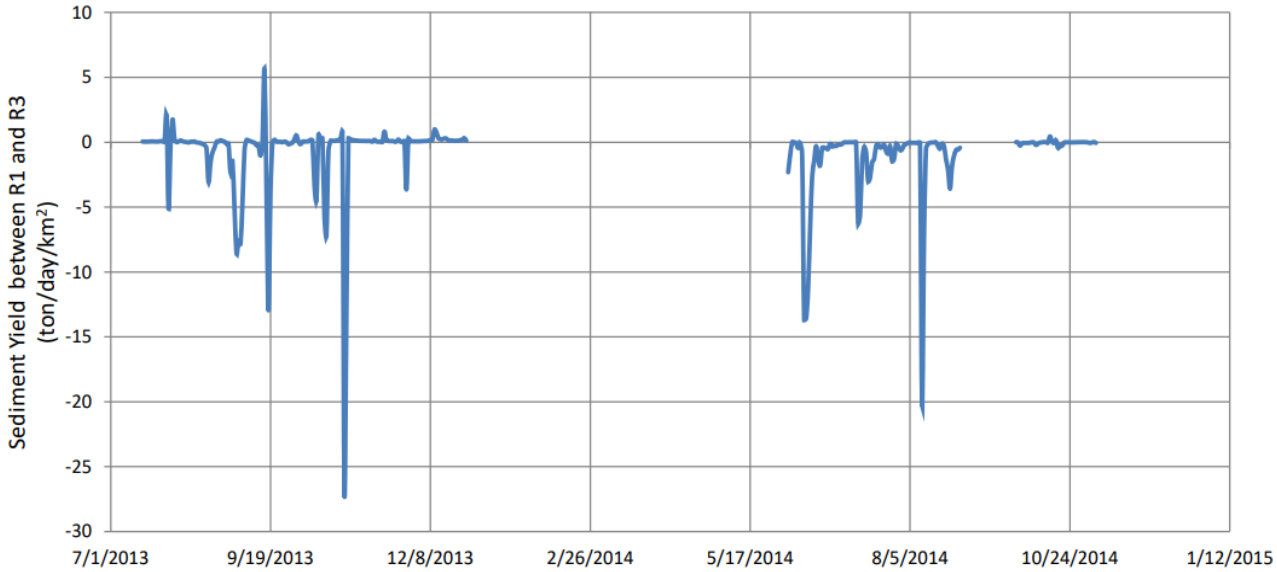

Figure 11. Sediment yield between site R1 and site R2.

grassland. Thus, the sediment availability by soil erosion is probably very low. Thus, most of the suspended sediment originates in the upstream of site R2 and partly deposits between site R1 and site R2.

4.5. Sediment Load in Different Subbasins by SWAT

The Oikamanai River catchment was divided into 3 subbasins (Figure 4(a)) based on water divide, soil type, land use and slope classes for the tributaries upstream of site R1. The SWAT model simulated the sediment load at every subbasin (Figure 12). It is seen that the sediment load and sediment yield at subbasin 2 (Figure 12(a) and Figure 12(b)) is at any time greater than that in subbasin 1 or subbasin 3, and that at most of the time the sediment yield in subbasin 3 is negative (Figure 12(c)). The net sediment yield in subbasin 3 was calculated by (R1 sediment load – R2 sediment load)/(Area between R1 and R2) (Figure 10). A similar scenario was also seen in the observed data (Figure 11), where the

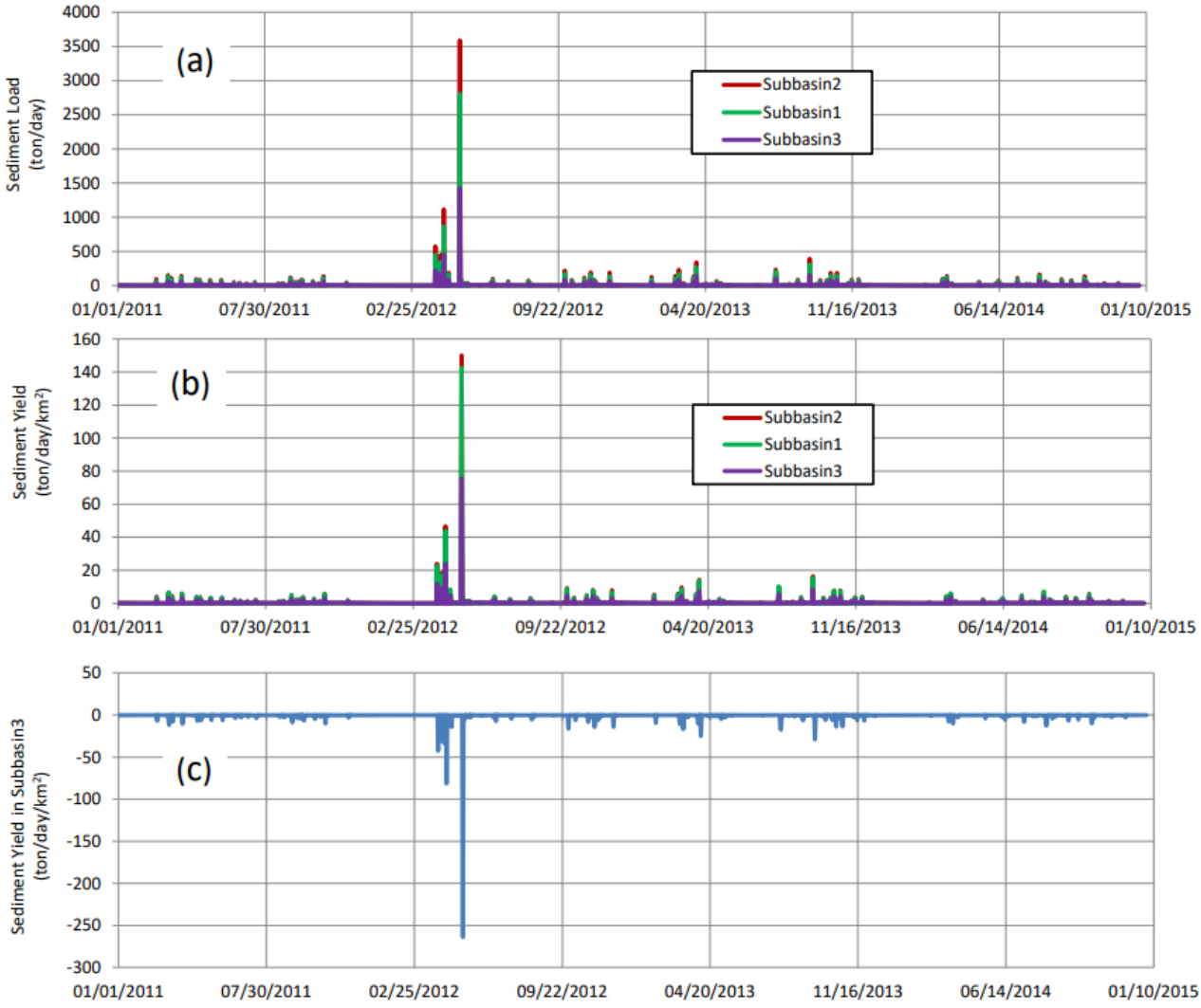

Figure 12. Sediment load and sediment yield calculated in the three subbasins. (a) sediment load and (b) sediment yield in three subbasins, and (c) calculated net sediment yield in subbasin 3.

sediment deposition occurred between site R2 and site R1.

5. Conclusion

Hourly and daily time series of discharge, suspended sediment concentration and sediment load were obtained in the forested Oikamanai River catchment influenced by the slope failure. The observed and SWAT-simulated outputs definitely showed that subbasin 2 in **Figure 4(a)** is the main sediment source in this study area (**Figure 12**). Part of suspended sediment deposits between sites R2 and R1, since the sediment yield at site R2 is at any time greater than at site R1. This reflects the frequent occurrence of landslide and bank collapse upstream of site R2, following rainfalls onto the catchment slope and the riparian region in the tectonically active forested catchment. A definitive interpretation of the quantitative results is not yet appropriate, because some processes are not well presented in the SWAT model and the lack of model parameterization at a local scale. While this study is able to give relative estimates of erosion measures, further model parameterization at a local scale should be done as more data and more information become available.

Acknowledgements

We are indebted to the Government of the Taiki-city and Fishermen's Union at Hama-Taiki Village for their kind permission of our field observations in the Oikamanai River. We express our gratitude to the farmers, Messrs. Mori and Takahashi, at the Seika Village for their frequent water sampling and instrument management. This study was supported partly by the Grant for Joint Research Program of the Institute of Low Temperature Science, Hokkaido University.

Conflicts of Interest

The authors declare no conflicts of interest regarding the publication of this paper.

References

[1] Cao, C., Feng, J. and Tao, Z. (2020) Start-Up Mechanism and Dynamic Process of Landslides in the Full High Waste Dump. *Water*, **12**, 2543. https://doi.org/10.3390/w12092543

[2] Teng, T.-Y., Huang, J.-C., Lee, T.-Y., Chen, Y.-C., Jan, M.-Y. and Liu, C.-C. (2020) Investigating Sediment Dynamics in a Land-Slide-Dominated Catchment by Modeling Landslide Area and Fluvial Sediment Export. *Water*, **12**, 2907. https://doi.org/10.3390/w12102907

[3] Armoza-Zvuloni, R., Shlomi, Y., Abadi, I., Shem-Tov, R. and Laronne, J.B. (2022) Fluvial Sediment Yields in Hyper-Arid Areas, Exemplified by Nahal Nehushtan, Israel. *Land*, **11**, 1050. https://doi.org/10.3390/land11071050

[4] Najib, S., Aliah, S. and Hamidon, H. (2020) Suspended Sediment Concentration and Sediment Loading of Bernam River (Perak, Malaysia). *Transylvanian Review of Systematical and Ecological Research*, **22**, 1-14. https://doi.org/10.2478/trser-2020-0007

[5] Asselman, N.E.M. (1999) Suspended Sediment Dynamics in a Large Drainage Basin: The River Rhine. *Hydrological Processes*, **13**, 1437-1450. https://doi.org/10.1002/(SICI)1099-1085(199907)13:10<1437::AID-HYP821>3.0.CO;2-J

[6] McCullough, M.C., Eisenhauer, D.E. and Dosskey, M. (2008) Modeling Runoff and Sediment Yield from a Terraced Watershed Using WEPP. USDA Forest Service/UNL Faculty Publications, Paper No. MC08-118, University of Nebraska, Lincoln, 12 p.

[7] Qiu, L., Zheng, F. and Yin, R. (2012) SWAT-Based Runoff and Sediment Simulation in a Small Watershed, the Loessial Hilly-Gullied Region of China: Capabilities and Challenges. *International Journal of Sediment Research*, **27**, 226-234. https://doi.org/10.1016/S1001-6279(12)60030-4

[8] Araiba, K., Nozaki, T., Jeong, B. and Fukumoto, Y. (2008) Distribution of Landslides and Their Geological Characteristics in Japan. *Journal of the Japan Landslide Society*, **44**, 37-44. https://doi.org/10.3313/jls.44.318

[9] Ndomba, P. (2015) Validation of GLASOD Map for Sediment Sources and Erosion Processes Identification in the Nyumba Ya Mungu Reservoir Catchment. *International Journal of Geosciences*, **6**, 972-986. https://doi.org/10.4236/ijg.2015.69077

[10] Nasirzadehdizaji, R. and Akyuz, D.E. (2022) Application of Swat Hydrological Model to Assess the Impacts of Land Use Change on Sediment Loads. *Journal of Agriculture, Environment and Food Sciences*, **6**, 108-120. https://doi.org/10.31015/jaefs.2022.1.15

[11] Talebizadeh, M., Morid, S., Ayyoubzadeh, S.A. and Ghasemzadeh, M. (2010) Uncertainty Analysis in Sediment Load Modeling Using ANN and SWAT Model. *Water Resources Management*, **24**, 1747-1761. https://doi.org/10.1007/s11269-009-9522-2

[12] Oeurng, C., Sauvage, S. and Sanchez-Perez, J.M. (2011) Assessment of Hydrology, Sediment and Particulate Organic Carbon Yield in a Large Agricultural Catchment Using the SWAT Model. *Journal of Hydrology*, **401**, 145-153. https://doi.org/10.1016/j.jhydrol.2011.02.017

[13] Mukundan, R., Radcliffe, D.E. and Risse, L.M. (2010) Spatial Resolution of Soil Data and Channel Erosion Effects on SWAT Model Predictions of Flow and Sediment. *Journal of Soil and Water Conservation*, **65**, 92-104. https://doi.org/10.2489/jswc.65.2.92

[14] Chu, T.W., Shirmohammadi, A., Montas, H. and Sadeghi, A. (2004) Evaluation of the SWAT Model's Sediment and Nutrient Components in the Piedmont Physiographic Region of Maryland. *Transactions of the ASAE*, **47**, 1523-1538. https://doi.org/10.13031/2013.17632

[15] Saghafian, B., Sima, S., Sadeghi, C. and Jeirani, F. (2012) Application of Unit Response Approach for Spatial Prioritization of Runoff and Sediment Sources. *Agricultural Water Management*, **109**, 36-45. https://doi.org/10.1016/j.agwat.2012.02.004

[16] Chikita, K.A., Iwasaka, W., Mamun, A.A., Ohmori, K. and Itoh, Y. (2012) The Role of Groundwater Outflow in the Water Cycle of a Coastal Lagoon Sporadically Opening to the Ocean. *Journal of Hydrology*, **464-465**, 423-430. https://doi.org/10.1016/j.jhydrol.2012.07.035

[17] Chikita, K.A., Uyehara, H., Mamun, A.A., Pascalis, F.D., Umgiesser, G., Iwasaka, W., Hossain, D.M. and Sakata, Y. (2015) Water and Heat Budgets in a Coastal Lagoon Controlled by Groundwater Outflow to the Ocean. *Limnology*, **16**, 149-157.

https://doi.org/10.1007/s10201-015-0449-4

[18] Hossain, M.M., Chikita, K.A., Sakata, Y., Miyamoto, T. and Ochiai, Y. (2015) Groundwater Leakage and River Runoff in a Catchment Influenced by Tectonic Movement. *Open Journal of Modern Hydrology*, **5**, 32-44. https://doi.org/10.4236/ojmh.2015.52004

[19] Miyamoto, T., Chikita, K.A., Sakata, Y., Ochiai, Y., Hossain, M.M., Oyagi, H. and Kudo, I. (2016) Loading Processes of Major Ions in a Forested Catchment: Observations and Modelling. *Journal of Japanese Association of Hydrological Sciences*, **46**, 39-57. https://doi.org/10.4145/jahs.46.39

[20] Arnold, J.G., Srinivasan, R., Muttiah, R.S. and Williams, J.R. (1998) Large Area Hydrologic, Modeling and Assessment Part I: Model Development. *JAWRA Journal of the American Water Resources Association*, **34**, 73-89. https://doi.org/10.1111/j.1752-1688.1998.tb05961.x

[21] Neitsch, S.L., Arnold, J.G., Kiniry, J.R., Williams, J.R. and King, K.W. (2005) Soil and Water Assessment Tool. Theoretical Documentation, Version 2005. TWRI TR-191. Texas Water Resources Institute, College Station, 476 p.

[22] US Department of Agriculture—Soil Conservation Service National Engineering Handbook, Section IV (1972) Hydrology, 4-102.

[23] Green, W.H. and Ampt, C.A. (1911) Studies on Soil Physics: I. Flow of Air and Water through Soils. *The Journal of Agricultural Science*, **4**, 1-24. https://doi.org/10.1017/S0021859600001441

[24] Arnold, J.G., Williams, J.R. and Maidment, D.R. (1995) Continuous Time Water and Sediment Routing Model for Large Basins. *Journal of Hydraulic Engineering*, **121**, 171-183. https://doi.org/10.1061/(ASCE)0733-9429(1995)121:2(171)

[25] Priestley, C. and Taylor, R. (1972) On the Assessment of Surface Heat Flux and Evaporation Using Large-Scale Parameters. *Monthly Weather Review*, **100**, 81-92. https://doi.org/10.1175/1520-0493(1972)100<0081:OTAOSH>2.3.CO;2

[26] Monteith, J.L. (1965) Evaporation and Environment. *Symposia of the Society for Experimental Biology*, **19**, 205-234.

[27] Hargreaves, G., Hargreaves, G. and Riley, J. (1985) Agricultural Benefits for Senegal River Basin. *Journal of Irrigation and Drainage Engineering*, **111**, 113-124. https://doi.org/10.1061/(ASCE)0733-9437(1985)111:2(113)

[28] Williams, J.R. (1969) Flood Routing with Variable Travel Time or Variable Storage Coefficients. *Transactions of the ASAE*, **12**, 100-103. https://doi.org/10.13031/2013.38772

[29] Chow, V.T. (1959) Open Channel Hydraulics. McGraw-Hill Book Company, New York, 700 p.

[30] Williams, J.R. (1975) Sediment Routing for Agricultural Watersheds. *JAWRA Journal of the American Water Resources Association*, **11**, 965-974. https://doi.org/10.1111/j.1752-1688.1975.tb01817.x

[31] Williams, J. and Berndt, H. (1977) Sediment Yield Prediction Based on Watershed Hydrology. *Transactions of the ASAE*, **20**, 1100-1104. https://doi.org/10.13031/2013.35710

[32] Williams, J. (1980) SPNM, a Model for Predicting Sediment, Phosphorus, and Nitrogen Yields from Agricultural Basins. *JAWRA Journal of the American Water Resources Association*, **16**, 843-848. https://doi.org/10.1111/j.1752-1688.1980.tb02497.x

[33] Nash, J.E. and Sutcliffe, J.V. (1970) River Flow Forecasting through Conceptual

Models. Part 1: A Discussion of Principles. *Journal of Hydrology*, **10**, 282-290. https://doi.org/10.1016/0022-1694(70)90255-6

[34] Santhi, C., Arnold, J.G., Williams, J.R., Dugas, W.A., Srinivasan, R. and Hauck, L.M. (2001) Validation of the SWAT Model on a Large River Basin with Point and Nonpoint Sources. *JAWRA Journal of the American Water Resources Association*, **37**, 1169-1188. https://doi.org/10.1111/j.1752-1688.2001.tb03630.x

[35] Abbaspour, K.C. (2007) User Manual for SWAT-CUP, SWAT Calibration and Uncertainty Analysis Programs. Eawag: Swiss Federal Institute of Aquatic Science and Technology, Duebendorf, 103 p.

[36] Arnold, J.G., Moriasi, D.N., Gassman, P.W., Abbaspour, K.C., White, M.J., Srinivasan, R. and Jha, M.K. (2012) SWAT: Model Use, Calibration, and Validation. *Transactions of the ASAE*, **55**, 1491-1508. https://doi.org/10.13031/2013.42256

[37] Phomcha, P., Wirojanagud, P., Vangpaisal, T. and Thaveevouthti, T. (2011) Predicting Sediment Discharge in an Agricultural Watershed: A Case Study of the Lam Sonthi Watershed, Thailand. *Science Asia*, **37**, 43-50. https://doi.org/10.2306/scienceasia1513-1874.2011.37.043

[38] Kim, J.G., Park, Y.S., Yoo, D., Kim, N., Engel, B.A., Kim, S., Kim, K.S. and Lim, K.J. (2009) Development of a SWAT Patch for Better Estimation of Sediment Yield in Steep Sloping Watersheds. *JAWRA Journal of the American Water Resources Association*, **45**, 963-972. https://doi.org/10.1111/j.1752-1688.2009.00339.x

[39] Babel, M.S., Shrestha, B. and Perret, S. (2011) Hydrological Impact of Biofuel Production: A Case Study of the Khlong Phlo Watershed in Thailand. *Agricultural Water Management*, **101**, 8-26. https://doi.org/10.1016/j.agwat.2011.08.019